Impact of Oxygen Transport Properties on Polypropylene Thermal Oxidation, Part 1: Effect of Oxygen Solubility

Alexandre François-Heude,[1,2] Emmanuel Richaud,[1] Alain Guinault,[1] Eric Desnoux,[2] Xavier Colin[1]
[1]Arts et Metiers ParisTech, PIMM Laboratory (CNRS UMR 8006), Paris, France
[2]Renault, DETC-A department, Guyancourt, France
Correspondence to: A. François-Heude (E-mail: Alexandre.FRANCOIS-HEUDE@ensam.eu)

ABSTRACT: A general kinetic model is proposed to describe the polypropylene thermal oxidation of thin polypropylene films in a wide range of temperatures (from 60 to 200°C) and oxygen partial pressures (from 0.02 to 5 MPa) using a single set of parameters. This model was calibrated with several series of experimental data including analyses of primary (hydroperoxides) and secondary oxidation products (carbonyl species), and subsequent changes in macromolecular properties (average molecular masses). It predicts the experimental data previously published in the literature in terms of induction times and maximal oxidation rates. The variability of the oxygen solubility coefficient allows to explain the scattering of induction times and oxidation rates among the whole iPP family, but also the dependence of this latter quantity with oxygen partial pressure. This variability is presumably due to iPP polymorphism in the temperature range where oxygen permeability is commonly measured. It is concluded that the kinetic model can be used to study the direct effect of iPP morphology on its thermal oxidation kinetics (chemistry of oxidation). © 2014 Wiley Periodicals, Inc. J. Appl. Polym. Sci. **2014**, *132*, 41441.

KEYWORDS: degradation; kinetics; morphology; polyolefins

INTRODUCTION

In the early 1990s, a formal kinetic approach, which consists in focusing on the critical oxidation path, that is to say basing on the rate determining step, was proposed at the laboratory in order to get around the overcomplexity of radical chain oxidation mechanisms. The main propagation product: hydroperoxide, was shown to be the key initiating species. Indeed, its decomposition leads to the generation of a vast majority of alkyl and peroxy radicals then reacting with oxygen. This closed-loop character was shown to well describe the auto-accelerated behavior of polypropylene thermal oxidation from the end of the induction period.[1]

From this standpoint, major advances were made in kinetic modeling. Efforts were brought about the eradication of the usual simplifying hypotheses (long oxidation kinetic chains, Bodenstein-Semenov steady-state, oxygen excess, and existence of an interrelationship between termination rate constants), which are necessary for any analytical treatment, but lead to serious inaccuracies when results have to be extrapolated to longer times or lower temperatures. This first numerical model[2] enabled to simulate accurately the control of oxidation kinetics by oxygen diffusion. It substantiated the overall consistency of the postulated mechanistic scheme, but the kinetic rate constants were mainly estimated from model compounds. Further developments were about the impact of oxygen partial pressure on polypropylene thermal oxidation kinetics at solid[3] and molten states.[4] In both cases, the rate constants were determined by applying an inverse resolution method in order to facilitate the model convergence with a unique set of parameters values, as done successfully for instance for polyethylene.[5] This approach has been generalized in our laboratory to determine all the unknown parameters, essentially rate constants, for a given kinetic model, and to simulate the experimental results with minimum deviation. If not possible, the postulated mechanistic scheme and the corresponding kinetic model are progressively complexified by adding stepwise new elementary reactions, and the parameters values are readjusted through a trial and error procedure.

Despite these encouraging results, this approach seems to have limitations, in particular in the controversial case of isotactic polypropylene (iPP). Indeed, reading of previous kinetic literature works, it turns out to be impossible to converge toward a unique set of parameters values, which raises the question of the model "universality" in respect with the wide scattering of thermal oxidation behaviors among the whole iPP family. This

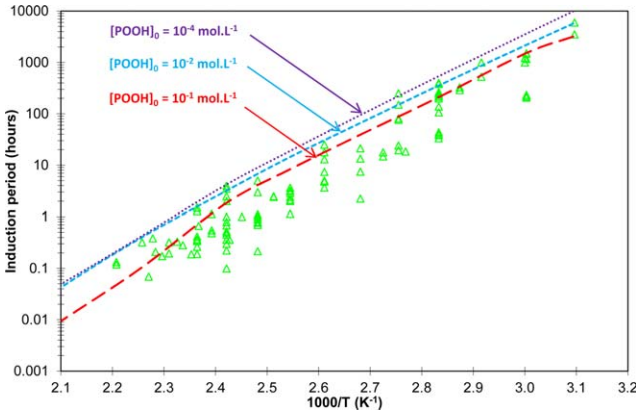

Figure 1. Arrhenius plot of the oxidation induction times compiled from the literature between 50 and 190°C in air. Dotted lines: simulations made with the kinetic model described in Ref. 3 for various values of $[POOH]_0$ (and a unique value of solubility of 4.2×10^{-7} exp (−6700/RT) mol L^{-1} Pa^{-1}. Symbols (△): compilation of literature data measured by oxygen uptake, carbonyl index, microcalorimetry, or chemiluminescence in air. [Color figure can be viewed in the online issue, which is available at wileyonlinelibrary.com.]

apparent variability has been largely attributed to the presence of impurities or structural defects such as catalysis residues, traces of stabilizers, chemical irregularities (including oxidation products) generated during processing or storage.[6,7] All these defects are in a very low concentration, analytically out of reach, and thus are currently assimilated to an initial concentration of hydroperoxides $[POOH]_0$ as adjustable parameter.[8] This quantity represents a hypothetical (but kinetically equivalent) value accounting for all the radical-producing species initially present into the polymer sample. Indeed, all these extrinsic sources of radicals are expected to vanish while hydroperoxides accumulate in the early periods of exposure, thus becoming quickly negligible compared to hydroperoxides decomposition. $[POOH]_0$ values, usually ranged between 10^{-5} and 10^{-1} mol L^{-1}, were shown to describe properly the scattering of induction times for polyethylene which spreads over only one decade.[9,10] The upper limit (10^{-1} mol L^{-1}) would simply correspond to the threshold above which the polymer samples could be considered "dirty" and thus, should be rejected. In comparison, iPP induction times[11–20] range over two decades (Figure 1) and thus, cannot be fully described by such a variation range of $[POOH]_0$. This result may suggest additional sources of variabilities, which will be tentatively elucidated in this study.

The objective of this article is to consider the crystalline morphology as another source of variability, which could affect oxygen transport properties, in particular oxygen solubility. Of course, such an assumption will be considered as satisfactory only if it allows modeling all the thermal oxidation behaviors among the whole iPP family with a single set of parameters values.

EXPERIMENTAL

Materials

A reference iPP, supplied by Aldrich (ref. 427888) as pellets and denoted iPP1, has been chosen for this study to properly calibrate the kinetic model. Its thermo-oxidative behavior has been compared with those previously reported in the literature for two other iPPs, denoted iPP2 and iPP3.[3,12] Their respective physicochemical characteristics are reported in Table I.

IPP1 films of 80–130 μm thick were obtained by compression molding with a Gibitre laboratory press under a pressure of 20 MPa during 30 s at 200°C. Additives were removed by Soxhlet extraction for 48 h using dichloromethane as solvent without altering the film integrity. The crystallinity was found equal to 45 ± 3 wt % by Differential Scanning Calorimetry (TA Q1000 apparatus) taking a melting enthalpy for crystalline lamellae of $\Delta H_m^0 = 209$ J/g.

Thermal Aging Conditions and FTIR Aging Monitoring

iPP1 samples were thermally aged at temperatures ranged between 60 and 140°C in air-ventilated ovens regulated at ±1°C. Aging monitoring was done with a Perkin-Elmer FTIR spectrophotometer (16 scans, resolution 4 cm^{-1}), basing on the peak of carbonyls at 1713 cm^{-1} ($\varepsilon = 300$ L mol^{-1} cm^{-1}). Low residual concentrations of stabilizers may induce a significant scattering on data between different batches of purification. As a consequence, we proceeded in two steps. First, films stemming from a single batch were submitted to a nondestructive FTIR monitoring at 60, 70, 80, 90, 100, 120, and 140°C in air. These results were considered as standards (as a kind of calibration curve depending on temperature) to correct the statistical bias in terms of induction times (due to the presence of stabilizer residues) for the subsequent destructive analyses on films coming from other batches.

Characterization by Complementary Destructive Analyses

The iodine method was chosen to perform hydroperoxides titration, instead of the sulfide dioxide or ferrous cyanate reactive methods, due to its better reliability for polypropylene.[21,22]

Table I. Specifications of Investigated iPPs

Material	Reference iPP1	iPP2[3]	iPP2[12]
Supplier/grade	Aldrich	BIDIM geosynthetics	Montell/Profax 6501
MFI [230°C, 2.16 kg] (g/10 min)	12	-	4
Mw (kg mol^{-1})	250	170	165
Mn (kg mol^{-1})	67	70	44
Polydispersity index	3.7	2.5	3.8
Crystallinity ratio (wt %)	45	35	50

Table II. Coefficients Used for Universal Calibration

Materials	K (10^3 mL g^{-1})	α	References
Polystyrene standards	13.8	0.70	124,125
Polypropylene	15.2	0.76	126

This former is based on the reduction of hydroperoxides by sodium iodide in an acidic medium according to the reaction:

$$R_3COOH + 3I^- + 2H^+ \rightarrow R_3COH + I_3^- + H_2O$$

The concentration of I_3^- ions was titrated by UV spectrophotometry at 355 nm using a Perkin-Elmer Lambda 35 device and a molar extinction coefficient of $\varepsilon = 25{,}000$ L mol^{-1} cm^{-1}. About 10 mg of PP sample and 7 mL of a solution of isopropanol and acetic acid solvents mixture (10 : 1) were introduced into a two neck glass flask equipped with a bulb condenser. When refluxing, 2 mL of sodium iodide dissolved in isopropanol (200 g/L) was added with a syringe throughout the side neck. After 10 min, the mixture was quenched up to room temperature with 25 mL of distilled water. It is noteworthy that the previous iodometry procedure does not enable discrimining between hydroperoxides, peracids, and peresters. Dialkyl peroxides would not be titrated in theory except if hydrochloric acid is used instead of acetic acid as catalyst. The accuracy on concentration measurement was estimated to be ± 7.5 mol %.

Molecular Weight Measurements

Gel Permeation Chromatography (GPC) experiments were performed with a PL-GPC 220 high temperature device commercialized by Agilent Technologies. The GPC was equipped with a guard column and two columns branded PLGel Olexis as well as a refractive index detector. The eluent was 1,2,4-trichlorobenzene (Chromasolv, Sigma-Aldrich) stabilized with 0.03 wt % of 2,6-di-*tert*-butyl-4-methylphenol (BHT, Fluka). It was filtered with a 0.2 μm pore size membrane (in PTFE, Whatman) before use. The injection volume was 200 μL and the flow rate was 1.0 mL/min. PP samples were dissolved in 1,2,4-trichlorobenzene/BHT (0.3 wt %) using a PL-SP 260-VS high temperature sample preparation system (PL Ltd.) at 135°C during 20 min. The calibration curve was established from four Polystyrene Shodex narrow standards of respective molecular weights of 1,470,000, 257,000, 46,500 and 7,210 g mol^{-1}. Results were then corrected using the so-called "universal calibration", based on the well-known Mark-Houwink's relationship [eq. (1)] with the coefficient values reported in Table II.

$$[\eta] = K \cdot M^{\alpha} \quad (1)$$

Oxygen Permeability

Oxygen permeability measurements were performed with a Systech 8001 device on films of about 130 μm thick at 10, 23, or 45°C and 0% of relative humidity. Their active surface area was equal to 50 cm^2. The time-lag method was chosen to measure oxygen transport properties (see for instance Ref. 23). This analysis mode required a complete purge of the system (including detector, pipes, and samples) under a pure nitrogen flow, up to 0.4 ppm as baseline, prior to introduce pure oxygen gas. The diffusivity can be calculated by intercepting with the x-abscissa the straight-line describing the steady-state regime of the kinetic curve of oxygen cumulated amount Q_{O2} obtained by integrating the kinetic curve of Oxygen Transmission Rate along time. For a semi-infinite film of thickness L, this straight-line obeys the following general equation:

$$Q = \alpha\left(t - \frac{L^2}{6D_{O_2}}\right) \quad (2)$$

where α is a constant.

Therefore, the oxygen diffusivity D_{O_2} is given by:

$$D_{O_2} = \frac{L^2}{6t_{Q=0}} \quad (3)$$

where $t_Q = 0$ is the time-lag.

The oxygen solubility S_{O_2} is related to the oxygen diffusivity D_{O_2} and permeability Pe_{O_2} according to:

$$S_{O_2} = {}^{D_{O_2}}\!/_{Pe_{O_2}} \quad (4)$$

THEORY OF FORMAL KINETIC MODELING

Closed-Loop Mechanistic Scheme

Most of the mechanistic schemes, used as basis to describe the general trends of oxidation kinetics, were derived from the standard scheme proposed by Bolland and Gee for ethyl linoeate[24] and then, extended to saturated and unsaturated hydrocarbon polymers, namely polyolefins and elastomers.[25,26] As a general strategy, this scheme was progressively complexified by adding a minimal number of reactions to minimize the number of adjustable parameters, thus facilitating analytical or numerical solving. This strategy of formal kinetic (just like the versatile Tobolsky's model proposed in the 1950's which used a reduced number of parameters in Refs. 27 and 28) differs from the approach adopted by Somersall and Guillet,[29] whose mechanistic scheme included all the elementary reactions involved in the aging process. The resulting Closed-Loop Mechanistic Scheme (CLMS) for polypropylene is given below with the rate constants k_i relative to each step:

Initiation

(1u) $POOH \rightarrow 2P^{\bullet} + (1-\gamma_1)POH + \gamma_1 P{=}O + H_2O + \gamma_s S \quad (-2PH) \quad (k_{1u})$

(1b) $2POOH \rightarrow P^{\bullet} + PO_2^{\bullet} + (1-\gamma_1)POH + \gamma_1 P{=}O + H_2O + \gamma_s S \quad (-PH) \quad (k_{1b})$

Propagation

(2) $P^{\bullet} + O_2 \rightarrow PO_2^{\bullet} \qquad (k_2)$

(3) $PO_2^{\bullet} + PH \rightarrow POOH + P^{\bullet} \qquad (k_3)$

Termination

(4) $P^{\bullet} + P^{\bullet} \rightarrow \gamma_4 P{-}P + (1-\gamma_4)PH + (1-\gamma_4)F + \gamma_4 B \qquad (k_4)$

(5) $P^{\bullet} + PO_2^{\bullet} \rightarrow \gamma_5 POOP + (1-\gamma_5)POOH + (1-\gamma_5)F + \gamma_5 B \quad (k_5)$

(6a) $PO_2^{\bullet} + PO_2^{\bullet} \rightarrow \left[PO^{\bullet\bullet}OP\right]_{cage} + O_2 \quad (k_{6a})$

(6b) $\left[PO^{\bullet\bullet}OP\right]_{cage} \rightarrow POOP + B \quad (k_{6b})$

(6d) $\left[\mathrm{PO^{\cdot}\cdot OP}\right]_{\mathrm{cage}} \rightarrow 2\mathrm{P^{\cdot}} + 2(1-\gamma_1)\mathrm{POH} + 2\gamma_1\mathrm{P{=}O} + 2\gamma_s\mathrm{S} \quad (-2\mathrm{PH}) \quad (k_{6d})$

with the following formalism:

- PH accounts for tertiary CH groups,
- $\mathrm{P^{\cdot}}$, $\mathrm{PO_2^{\cdot}}$, $\mathrm{PO^{\cdot}}$ account respectively for alkyl, peroxy, and alkoxy radicals,
- POOH, POOP, P-OH, P=O account, respectively, for hydroperoxides, dialkyl peroxides, alcohols, and ketones as macromolecular oxidation products,
- γ_1 is the yield of β scission (leading to ketones), irrespectively of the molecularity of the initiation reaction, in competition with hydrogen abstraction (leading to alcohols):

$$\gamma_1 = \frac{k_{\beta\,\mathrm{scission}}}{k_{\beta\,\mathrm{scission}} + k_{\mathrm{H\,abstraction}}} \tag{5}$$

- γ_s is the yield in chain scission, which can differ from γ_1 since only β scission occurring on the main macromolecular chain would impact molecular masses contrary to scissions occurring on side-groups or chain extremities.
- From a practical point of view, it is more convenient to consider an apparent yield γ_1^{app} for carbonyl products owing to the high uncertainty on the nature of these species and the value of their corresponding molar extinction coefficients.
- γ_4 and γ_5 are the respective yields of alkyl-alkyl and alkyl-peroxy radicals coupling (of respective rate constants k_{4r} and k_{5r}), in competition with disproportionation (of respective rate constants k_{4d} and k_{5d}):

$$\gamma_4 = \frac{k_{4r}}{k_{4_r} + k_{4_d}} \tag{6}$$

and

$$\gamma_5 = \frac{k_{5r}}{k_{5_r} + k_{5_d}} \tag{7}$$

- F, S, and B account for double bonds, chain scissions and crosslinks (i.e. covalent bridges) respectively.
- Most of the justifications of these mechanistic considerations are detailed elsewhere,[4,30] but the fundamental principles and noticeable improvements of this model can be briefly detailed below:

i. The mechanistic scheme only considers a single reactive site: the methyne unit (tertiary CH groups);
ii. In terms of initiation processes, the hypothesis of a constant initiation rate (as considered, for instance, by Neiman and co. in Ref. 20 and reported by Reich and Stivala in Ref. 31) was dismissed in thermal oxidation, because it does not allow to simulate the induction period. In this latter case, the main source of radicals is the hydroperoxides decomposition whose molecularity was shown to be mainly bimolecular at temperatures typically lower than 200°C.[10] It is a balance reaction since the homolysis of the O—O bond is very slow and rate determining compared with the subsequent rearrangements of the very reactive alkoxy (PO•) and hydroxy ($\mathrm{HO^{\cdot}}$) radicals generated by this decomposition.
iii. In terms of termination reactions, recombinations of peroxy radicals were detailed taking into account their propagation outside the cage, as supported by the kinetic analyses made by Reich and Stivala.[31] Such a consideration aims at describing the mobility hindrance of peroxy macroradical when decreasing the temperature and thus, at predicting the change in kinetic regime below a critical temperature, located around 90°C for polyethylene.[32]
iv. Although the formation of volatile compounds (VOCs) is not explicited, it is taken into account through the apparent yield in carbonyl products γ_1^{app}.[33] It is important to remind here that the VOCs generation does not modify the polymer backbone since it takes place at the chain extremities. As a result, γ_s corresponds to the real yield of chain scissions in the middle-chain, which is responsible for the polymer embrittlement.

This general mechanistic scheme leads, by using the classical concepts of chemical kinetics, to a system of ordinary differential equations (SDE) describing the local concentration changes in primary products, that is to say $[\mathrm{P^{\cdot}}]$, $[\mathrm{PO_2^{\cdot}}]$, [POOH], $[\mathrm{PO^{\cdot}\cdot OP}]_{\mathrm{cage}}$, [PH] and $[\mathrm{O_2}]$, along the course of oxidation. These quantities are the most relevant to model because their calculation does not require the use of an additional apparent yield as adjustable parameter. Actually, only the concentrations of oxygen $[\mathrm{O_2}]$ and hydroperoxides [POOH] are currently measured. From a practical point of view, concentrations of secondary oxidation products, such as ketones, alcohols and related quantities (such as chain scissions S and crosslinking nodes B), are also very useful to check the model validity because they can be easily accessible experimentally. They are calculated in the post-treatment stage by integrating the following differential equations [eqs. (8)–(11)]:

$$\frac{d[\mathrm{C{=}O}]}{dt} = \gamma_1 k_{1u}[\mathrm{POOH}] + \gamma_1 k_{1b}[\mathrm{POOH}]^2 + 2\gamma_1 k_{6d}[\mathrm{PO^{\cdot}\cdot OP}] \tag{8}$$

$$\frac{d[\mathrm{OH}]}{dt} = (1-\gamma_1)k_{1u}[\mathrm{POOH}] + (1-\gamma_1)k_{1b}[\mathrm{POOH}]^2 + 2(1-\gamma_1)k_{6d}[\mathrm{PO^{\cdot}\cdot OP}] \tag{9}$$

$$\frac{dS}{dt} = \gamma_s k_{1u}[\mathrm{POOH}] + \gamma_s k_{1b}[\mathrm{POOH}]^2 + 2\gamma_s k_{6d}[\mathrm{PO^{\cdot}\cdot OP}] \tag{10}$$

$$\frac{dB}{dt} = \gamma_4 k_4[\mathrm{P^{\cdot}}]^2 + \gamma_5 k_5[\mathrm{P^{\cdot}}]\left[\mathrm{PO_2^{\cdot}}\right] + k_{6b}[\mathrm{PO^{\cdot}\cdot OP}] \tag{11}$$

For the full detail of the mathematical treatment, the reader is invited to refer to Appendix A. From both quantities S and B, subsequent multiscale properties can be then calculated, as for instance the decrease in weight M_w and number M_n average molecular masses by using the usual Saito's laws[34]:

$$\frac{S}{2} - 2B = \rho_{\mathrm{tot}}\left(\frac{1}{M_w} - \frac{1}{M_{\mathrm{w_O}}}\right) \tag{12}$$

and

$$S - B = \rho_{\mathrm{tot}}\left(\frac{1}{M_n} - \frac{1}{M_{\mathrm{n_O}}}\right) \tag{13}$$

where ρ_{tot} is the polymer density (0.91 g $\mathrm{cm^{-3}}$)

Strategy for the Optimization Procedure

According to the model previously described, the resolution of the chemical problem implies to determine up to 9 rate constants (k_{1u}, k_{1b}, k_2, k_3, k_4, k_5, k_{6a}, k_{6b} and k_{6d}) and 4 yields (γ_1^{app}, γ_4, γ_5 and γ_s) with their respective temperature dependences considering a reliable estimate of the initial concentration of hydroperoxides $[POOH]_0$. Moreover, literature data on rate constants k_2, k_4 and k_5 are very scarce because these latter are difficult to estimate independently. The problem could thus appear as underdetermined with such a high number of parameters, thus giving access to several numerically equivalent solutions, even if a large number of complementary experimental data is available.

Considering that an inverse resolution method may be tentatively used to solve this problem, the simpler the model will be, the better the problem will be conditioned. Therefore, to reduce the number of adjustable parameters, the strategy consists in oversimplifying the system, which can be conveniently operated by working at high oxygen partial pressure. Indeed, in such aging conditions, alkyl radicals $P^{\bullet}$ are rapidly converted into peroxy radicals $PO_2^{\bullet}$, so that the concentration in alkyl radicals is very low comparatively to the concentration in peroxy radicals.[3] In such a case, steps (4) (alkyl-alkyl radicals recombination) and (5) (alkyl-peroxy radicals recombination) can be neglected compared to step (6) (peroxy-peroxy radicals recombination).[3,5,31,35] This kinetic regime is called "oxygen excess", as the opposite of "oxygen default" conditions. Physically, the "oxygen excess" regime corresponds to the saturation of reactive sites (PH) by oxygen.

The optimization procedure thus first consists in determining the values of k_{1u}, k_{1b}, k_3, k_{6a}, k_{6b} and k_{6d} in oxygen excess. The value of k_3 was assumed to obey the semi-empirical Korcek's relationship.[36] Moreover, at high oxygen partial pressure, it can be assumed that $k_2[O_2]$ is much higher than $k_4[P^{\bullet}]$ or $k_5[PO_2^{\bullet}]$ (see invariant k_2/k_4 below). That is the reason why k_2 must be fixed in oxygen default as well as all other parameters neglected in oxygen excess, that is to say k_4, k_5, γ_4 and γ_5.

To facilitate the optimization of parameters determination, it is fruitful to understand their influence on the oxidation kinetics. In this perspective, kinetic relationships coming from the analytical solving are very valuable since providing a phenomenological description. They allow to understand the existence of some invariant quantities[5]:

1. In oxygen excess, the oxidation rate is maximal:

$$r_s = \frac{k_3^2[PH]^2}{4\,k_6} \tag{14}$$

The ratio k_3^2/k_6 describes the competition between the propagation by hydrogen abstraction (3) and bimolecular recombination of peroxy radicals (6).

2. The apparent rate constant k_6 describing the bimolecular recombination of peroxy radicals does not apply to an elementary step, but is the result of the combination of several competitive steps of termination into and outside the cage. The resulting relationship describing its non arrhenian behavior is[30,32]:

$$k_6 = \frac{k_{6a}}{\left(1+\frac{k_{6d}}{k_{6b}}\right)\left(1+\frac{k_{6d}}{2\,k_{6b}}\right)} \tag{15}$$

Thereby, the ratio k_{6d}/k_{6b} appears also as an invariant quantity.

3. The ratio k_2/k_4 was also reported as an invariant quantity resulting from the competition between very fast reactions involving alkyl radicals: oxygen addition (2) and bimolecular recombination (4).

Actually, the rate constant k_4 for alkyl-alkyl radicals recombination has almost no influence under the investigated conditions (at $P_{O2} = 0.02$ MPa). Thus, the latter invariant must be rather conceived as a constraint to preserve the heuristic value of the kinetic model, as well as the inequality postulated by Gillen and Clough, that is to say: $(k_5)^2 > 4\ k_4 \cdot k_6$.[37] This latter allows to fix the orders of magnitude of termination rate constants since it induces that $k_4 > k_5 >> k_6$ up to a temperature of about 160°C.

In a first approach, the yields γ_4 and γ_5 were fixed at zero for reporting results obtained in radio-oxidation[38] (since termination reactions are expected to be weakly impacted by ionizing radiations) to avoid the generation of an unrealistic crosslinking.

Therefore, the main challenge consists in the determination of the rate constant k_5 for alkyl-peroxy radical recombination (in consistency with previous literature data in Refs. 13, 38, and 39) which turns out to be closely interrelated with the values of oxygen solubility S_{O2} and rate constant k_2. A last invariant combination of rate constants can be deduced from the expression of the critical oxygen concentration above which oxygen is in excess in the sample:

$$[O_2]_c = {}^{K}\!/_{\beta} = K \cdot {}^{k_3\,k_5\,[PH]}\!/_{k_2\,k_6} \tag{16}$$

where K is an arbitrary value depending exclusively on the physical or chemical property under consideration (e.g. oxidation rate or induction time; see Appendix B).

Thus, the corresponding critical oxygen pressure is:

$$P_c = {}^{[O_2]_c}\!/_{S_{O_2}} = K \cdot {}^{k_3\,k_5\,[PH]}\!/_{k_2\,k_6\,S_{O_2}} \tag{17}$$

This last equation particularly evidences the existence of an interrelationship between the oxygen solubility and some kinetic rate constants, especially k_2 and k_5. Indeed, in oxygen default, the polymer is not saturated in oxygen anymore and the impact of oxygen solubility increases dramatically. A special interest was therefore dedicated to the determination of the oxygen transport properties, and to the estimation of their variability for the whole iPP family, prior to the calibration of k_5. Its accurate determination requires the knowledge of primary products concentrations, thus justifying additional experiments on the reference polypropylene (iPP1) such as hydroperoxides titration. This work is the result of an exhaustive back and forward procedure. For a sake of simplicity, the calibration of the model will be presented before investigating the effect of oxygen partial pressure.

MODEL CALIBRATION WITH IPP1 IN OXYGEN DEFAULT

Determination of the Oxygen Transport Properties

Since oxygen transport properties are suspected to impact the polypropylene oxidation behavior, the values of oxygen permeability, diffusivity, and solubility have been measured by permeametry on the reference isotactic polypropylene (iPP1) at 10, 23, and 45°C. Obviously, it would have been more relevant to measure directly these data over the higher temperature range investigated for aging, but it is unfortunately outside the device capacities. That is the reason why these three quantities were extrapolated at higher temperatures by assuming that they obey an Arrhenius' law.

In sufficiently thin iPP films (typically ~100 μm thick), thermal oxidation can be considered homogeneous in the whole thickness (no diffusion limited oxidation). Indeed, oxygen diffusion until the middle of samples is quasi instantaneous and thus, only the coefficient of oxygen solubility will be relevant for modeling thermal oxidation kinetics. That is the reason why only the value of oxygen solubility is given in this article whereas the values of oxygen permeability and diffusivity will be discussed in a future article dedicated to the determination of oxidation profiles in thicker iPP samples (typically few millimeters thick):

$$S_{O_2}^{tot} = 1.48 \cdot 10^{-6} \times \exp\left(-6700/RT\right) (\text{molL}^{-1}\text{Pa}^{-1}) \quad (18)$$

There is a large consensus in the literature on the fact that the oxygen solubility is proportional to the fraction of amorphous phase wherein oxygen is dissolved.[40] Thus, if S_{O2}^{am} and S_{O2}^{tot} are the respective oxygen solubilities in the amorphous phase and in the semicrystalline polymer, one can write:

$$S_{O_2}^{am} = \frac{S_{O_2}^{tot}}{1-\chi_c} \frac{\rho_{am}}{\rho_{tot}} \quad (19)$$

with χ_c the crystallinity ratio, ρ_{am} the density of the amorphous phase (0.85 g cm^{-3}) and ρ_{tot} the density of the semicrystalline polymer.

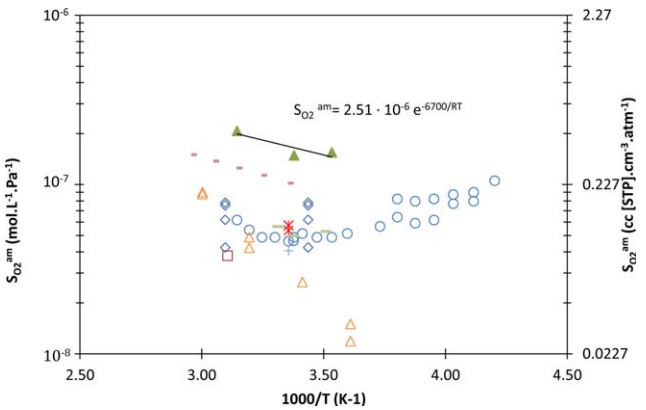

Figure 2. Comparison of the oxygen solubilities of iPPs measured in this study and compiled from the literature: ▲iPP1 (this study). ✳Lin et al.[45,46]; ○ Somlai et al.[47]; ▬ Villaluenga et al.[49]; ▬ Beltrame et al.[41]; ◇ Mani et al.[53]; ◇ Kiryushkin and coworkers[43,122]; □ Denisov and Afanas'ev[42]; + Thorlaksen et al.[48]; △ Kurek et al.[44] [Color figure can be viewed in the online issue, which is available at wileyonlinelibrary.com.]

Let us remind, here, that the chemical problem is solved in the amorphous phase and the structural changes in the semicrystalline polymer are deduced in a post-treatment stage [see eq. (A13) in Appendix A]. The values of oxygen solubility S_{O2}^{am} determined in the iPP amorphous phase in this study are compared with the data compiled from the literature[41–53] in Figure 2. S_{O2}^{am} is of the same order of magnitude and almost temperature independent for all iPPs. To illustrate, at 50°C, S_{O2}^{am} is ranged between $3 \cdot \times 10^{-8}$ and $2 \cdot \times 10^{-7}$ mol L^{-1} Pa^{-1}. Its activation energy is about 0 ± 5 kJ mol^{-1} for the whole literature dataset and 7 kJ mol^{-1} for iPP1 located in the upper range of the compilation.

Modeling the Changes in Primary Oxidation Products

Once the oxygen related parameters, in particular the coefficient of oxygen solubility, have been determined for the reference polypropylene (iPP1), it has been then possible to determine accurately the kinetic rate constants. The entire set of values able to describe the thermal oxidation behaviors of the three iPPs under study (iPPs 1, 2 and 3) is given in Table III.

These values result from the optimization procedure detailed in the previous section 'Strategy for the optimization procedure'. It is relevant to remind here that modeling the changes in hydroperoxides concentration was a key step in this study because it gives access to the value of k_5, which is closely related to the values of k_2 and S_{O2} (Figure 3).

Modeling the Build-Up of Secondary Oxidation Products

The simulation of the changes in carbonyls concentration is also satisfying (Figure 4), particularly when considering that a single apparent yield γ_1^{app} has been used for carbonyls over the whole temperature range under investigation at the solid state.

γ_1^{app} is prone to be dramatically impacted by:

1. the release of volatile compounds by the matrix, which are thereby not monitored,[33]
2. in a minor extent, the distribution of macromolecular oxidation products,
3. the changes in crystallinity ratio (for instance, due to annealing or chemicrystallization).

This parameter would be weakly temperature dependent, especially at temperatures lower than 140°C where VOC emissions would be noticeably low, which is rather beneficial for extrapolation at temperatures close to ambient. Moreover, the shape of the IR absorption band of carbonyl species remains unchanged when varying the temperature, which would confirm minor changes in the distribution of these species over the whole temperature range under study. In contrast, γ_1^{app} seems to depend more significantly on oxygen partial pressure, as discussed in "Discussion: towards a "universal" kinetic model."

Modeling the Changes in Average Molecular Masses

From the changes in macromolecular quantities, in particular chain scission and crosslink concentrations, it is possible to calculate the changes in weight M_w and number M_n average molecular masses according to the Saito laws [eqs. (12) and (13)]. The yield of chain scissions γ_s accounts for β-scissions occurring on the polymer middle chain and resulting in methyl ketones. In other words, β-scissions on side-chain methyl groups (responsible for

Table III. Arrhenius Parameters Used for Modeling Polypropylene Thermal Oxidation. k^0 and Ea Respectively Denote the Preexponential Factors and the Activation Energies

	k^0			
	iPP1	*iPP2*	*iPP3*	Ea (kJ mol^{-1})
$[POOH]_0$ (mol L^{-1})	4×10^{-3}	1×10^{-4}	1×10^{-4}	-
S_{O2}^{am} (mol L^{-1} Pa^{-1})	2.5×10^{-6}	4.2×10^{-7}	2.5×10^{-6}	6.7
D_{O2} (m^2 s^{-1})	8.7×10^{-6}	8.7×10^{-6}	8.7×10^{-6}	36.4
Pe_{O2} (cm^3 · cm · cm^{-2} · Pa^{-1} s^{-1})	2.9×10^{-6}	-	-	43.0
k_{1u} (s^{-1})[a]	2.9×10^{13}	1.9×10^{13}	2.9×10^{13}	140.7
		2.9×10^{13}		
k_{1b} (L mol^{-1} s^{-1})[b]	9.2×10^{8}	6.2×10^{8}	9.2×10^{8}	95.0
		9.2×10^{8}		
k_2 (L mol^{-1} s^{-1})	3.0×10^{9}	3.0×10^{9}	3.0×10^{9}	10.0
k_3 (L mol^{-1} s^{-1})	5.1×10^{7}	5.1×10^{7}	5.1×10^{7}	62.2
k_4 (L mol^{-1} s^{-1})	1.0×10^{12}	1.0×10^{12}	1.0×10^{12}	0.0
k_5 (L mol^{-1} s^{-1})	4.5×10^{10}	4.5×10^{10}	4.5×10^{10}	0.0
k_{6a} (L mol^{-1} s^{-1})	2.0×10^{17}	2.0×10^{17}	2.0×10^{17}	90.0
k_{6b} (s^{-1})	6.7×10^{6}	6.7×10^{6}	6.7×10^{6}	5.0
k_{6d} (s^{-1})	1.4×10^{12}	1.4×10^{12}	1.4×10^{12}	41.0
γ_1^{app}	0.5	0.5	0.5	-
γ_4	0	0	0	-
γ_5	0	0	0	-
γ_s	0.5	0.5	0.5	-

[a] $k_{1u}^0 = (2.4 \pm 1.5)\ 10^{13}$ s^{-1}.
[b] $k_{1b}^0 = (7.7 \pm 1.5)\ 10^{8}$ L mol^{-1} s^{-1}.

the generation of middle chain ketones) and chain extremities (volatile products) are not considered here.

Because of the large scattering of our experimental results, it was not possible to determine precisely a value for γ_s except at 100°C. Fortunately, values of this parameter were available in the literature.[13,54–58] This yield has been divided by the apparent yield in carbonyl species γ_1^{app}, calculated at the same temperature by neglecting the occurrence of crosslinks B in a first approach. Values of the ratio γ_s/γ_1^{app} for iPP, aPP (atactic polypropylene) and PE under various oxygen partial pressures between 90 and 160°C are reported in Table IV.

It can be seen that the mean value of γ_s/γ_1^{app} is around 0.8 for iPP (so $\gamma_s = 0.4$) whatever the temperature and the oxygen partial pressure. This value is slightly higher in PE (~1.2) and aPP

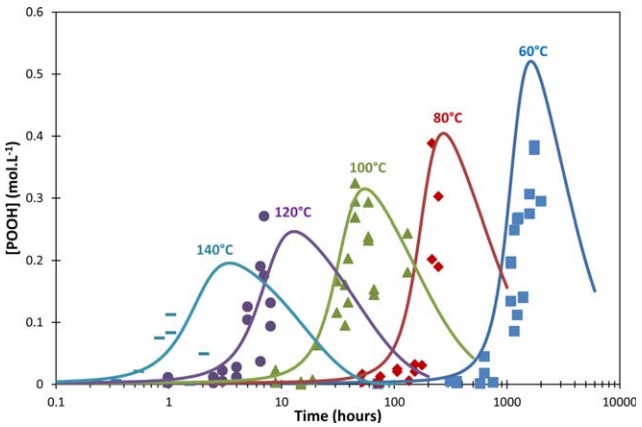

Figure 3. Changes in the hydroperoxydes concentration of iPP1 under 0.02 MPa between 60 and 140°C. Symbols: experimental data. Solid lines: kinetic modeling. [Color figure can be viewed in the online issue, which is available at wileyonlinelibrary.com.]

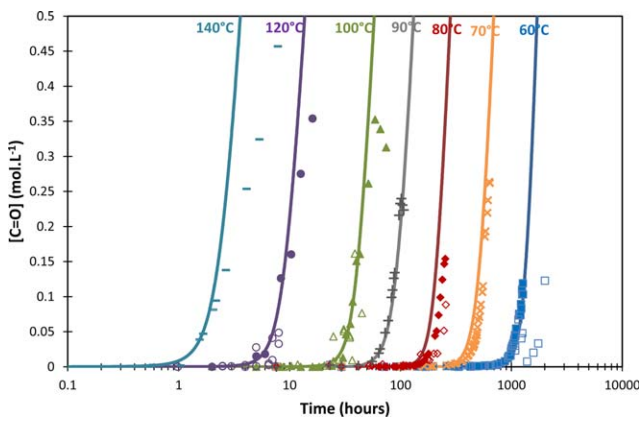

Figure 4. Changes in the carbonyls concentration of iPP1 under 0.02 MPa between 60 and 140°C. Symbols: experimental data. Solid lines: kinetic modeling. [Color figure can be viewed in the online issue, which is available at wileyonlinelibrary.com.]

Table IV. Ratio of the Yield in Chain Scission Over the Yield in Carbonyl Species Between 90 and 160°C Under Various Oxygen Partial Pressures for iPP, aPP and PE

P_{O2} (MPa)	T (°C)	Material	γ_s/γ_1^{app}	Reference
0.02	100	Bulk iPP	0.75	This study
0.01	130	Bulk iPP	0.99 ± 0.25	54
0.02	90	Bulk iPP	0.77	55
0.02	90-110	Bulk iPP	0.75 ± 0.15	13
1	130	Bulk iPP	0.67 ± 0.12	56
1	130	iPP in solution (0.56 mol L^{-1})	0.92 ± 0.23	56
0.02	120	Bulk aPP	0.78	57
1	130	Bulk aPP	1.20 ± 0.16	56
0.01	130	Bulk PE	1.42 ± 0.45	54
0.1	130-160	Bulk PE	0.99 ± 0.07	58

(~1.0). When considering the crosslinking reactions, the real yield in chain scissions for iPP is 0.5. The competition between chain scissions and crosslinking processes in iPP1 can be illustrated by the plot of $S = f(B)$ reported in Figure 5. The model generates a ratio S/B of 6 ± 2 in rather good agreement with the general experimental trend of 9.6 ± 2.7 evidenced on iPP1 in this study, but also on another iPP by Achimsky.[55]

In Figures 6 and 7, numerical simulations of M_n and M_w have been compared with experimental results. As expected [see eqs. (12) and (13)], M_w is more sensitive than M_n to crosslinking, which is materialized by the presence of an acute shoulder just before the drop of molecular masses. Thus, this observation is not a numerical artifact, but it is difficult to confirm experimentally because of the wide data scattering. Nevertheless, the model simulates the general experimental trend in the whole temperature range under study and confirms that chain scissions prevail largely over crosslinking whatever the temperature.

The ability of the model to predict the changes in macromolecular masses is highly valuable since the polypropylene lifetime, in terms of mechanical properties, can be determined according to a critical value of weight average molecular mass (end-of-life criterion).[59]

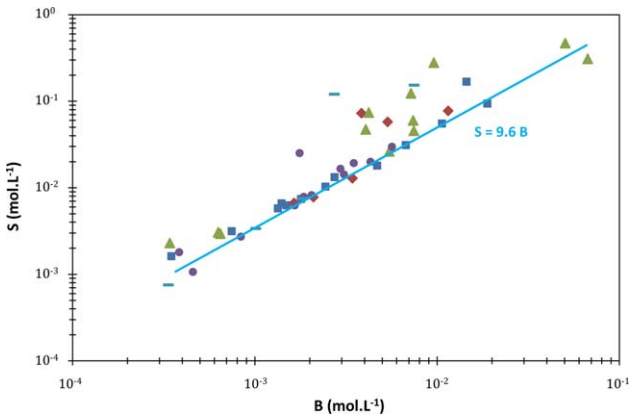

Figure 5. Number of chain scissions S versus number of crosslinks (or covalent bridges) B for iPP1 under 0.02 MPa between 60 and 140°C. Values of S and B have been obtained by solving the system of eqs. (8) and (9). Legend: ■ 60°C, ◆ 80°C, ▲100°C, ● 120°C, and ▬ 140°C. [Color figure can be viewed in the online issue, which is available at wileyonlinelibrary.com.]

DISCUSSION: TOWARDS A "UNIVERSAL" KINETIC MODEL

Common Sources of Variability in Connection with Initiation Processes

The optimization of parameters determination in oxygen excess, namely k_{1u}, k_{1b}, k_3, k_{6a}, k_{6b} and k_{6d}, was the first modeling stage of the polypropylene thermal oxidation. To be reliable, this optimization was mostly based on titration of hydroperoxides as primary oxidation products. Indeed, a lot of information is included in the shape of their concentration changes, focusing on the induction time, but also on the maximal and final concentrations. The shape of these curves, illustrating the autoaccelerated character of thermal oxidation, has been extendedly discussed elsewhere.[39] Figure 8 shows the best simulations used for determining the single set of parameters values (Table III).

According to assertions in "Strategy for the optimization procedure", in oxygen excess, the values of the coefficient of oxygen solubility and rate constant k_2 do not affect the oxidation kinetics. This is highly beneficial because the oxidation

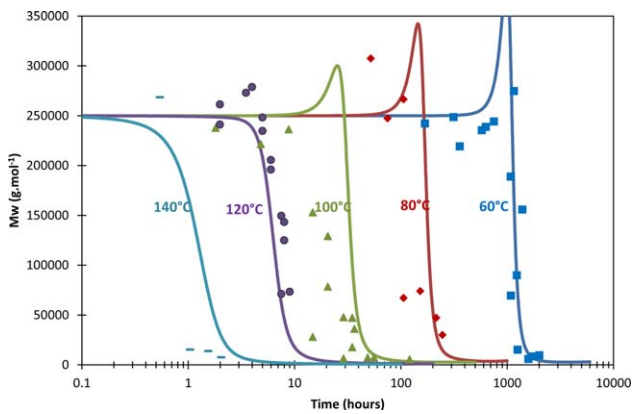

Figure 6. Changes in the weight average molecular mass of iPP1 under 0.02 MPa between 60 and 140°C. Symbols: experimental data. Solid lines: kinetic modeling. [Color figure can be viewed in the online issue, which is available at wileyonlinelibrary.com.]

behavior is not diffusion-controlled and so, independent of oxygen transport properties. Therefore, oxygen excess is particularly indicated to quantify the part of variability, which must be attributed to the multiplicity of initiating species, for example, chemical irregularities (including oxidized functions), traces of metal chelates, and residual concentration of stabilizers.

In this perspective, it is relevant to compare the oxidation behaviors of different iPPs under high partial oxygen pressure. Such experimental data have been advantageously collected from papers of Richaud et al. on iPP2[3] and Faulker on iPP3.[11] This latter turns out to have close morphological features and oxygen behavior with our reference material iPP1. That is the reason why the oxygen excess conditions have been considered as experimentally fulfilled for iPP1 under the highest oxygen partial pressure investigated by Faulkner (4.24 MPa) and Richaud et al. (5 MPa). This assumption will be checked later (see literature compilation of oxygen critical pressures in Figure 10).

Surprisingly, the discrepancies between the two kinds of polypropylenes cannot be described by a simple change in the initial concentration of hydroperoxides $[POOH]_0$, that is to say by a simple difference in their preoxidation state during processing and/or storage. It would thus require to adjust the initiation rate by slightly modifying the values of initiation rate constants (i.e. k_{1u}, k_{1b} or both). Metal particles are thought to favor unimolecular decomposition of hydroperoxides, but several arguments support the idea that the competition of both kinds of initiation processes would remain unchanged:

1. Modifying only k_{1u} would lead to a preexponential factor k^0_{1u} higher than the upper realistic value of 10^{13} s^{-1}.
2. The simulations show that the commonly accepted mechanism of hydroperoxides decomposition by catalyst residues (metal chelates)[60] partially behaves as a bimolecular process.
3. The bends of kinetic curves of carbonyl build-up at the end of the induction period are similar for the three different iPPs under investigation. This experimental observation suggests that the balance between both types of initiation processes must remain unchanged. In other words, the critical concentration in hydroperoxides $[POOH]_c$ must also remain unchanged[3,5] (this notion and its use in kinetic modeling is detailed in Appendix A):

$$[POOH]_c = \frac{k_{1u}}{k_{1b}} = \frac{k^0_{1u}}{k^0_{1b}} \exp\left(-\frac{E_u - E_b}{RT}\right) \quad (20)$$

In this study, a unique corrective factor (of 1.5) has been applied to k_{1u} and k_{1b} to report the observed discrepancies. This is eventually a moderate correction, which is not be sufficient to report the variability of induction times observed in oxygen default (Figure 1).

Such a behavior was previously evidenced by George and coworkers. They found that the amount of titanium catalyst has an impact on the pre-exponential factor of the Arrhenius law of induction time, but not on activation energy.[61–63] The effect of catalytic residues on the oxidation kinetics, already well-documented in the literature,[6,7] has been tested in a first approach. Although relevant to account for the variability of results in oxygen excess, this phenomenon is clearly insufficient to report for the oxidation behaviors of all iPPs in oxygen default.

Introduction of a Variability on the Coefficient of Oxygen Solubility

Dependences with Oxygen Partial Pressure. When buckling down to the kinetic modeling of thermal oxidation in oxygen default, the main issue was to explain the differences between the oxygen partial pressures dependences of induction times for the three iPPs under study, in particular iPP2 and iPP3 (knowing that iPP3 is characterized by similar features and oxidation behavior as iPP1). Indeed, in Figure 9, it is clear that these changes are less pronounced for iPP3 at 90°C than for iPP2 at 60, 80 or 100°C (for which they are rather homothetic). In other words, both types of iPP would have a different critical oxygen pressure.

According to our theoretical expectations [in particular from eq. (17)], this effect should be taken into account by adjusting the coefficient of oxygen solubility (rather than the rate constant k_5, which would constitute a physical nonsense for a given polymer family).

The changes in the carbonyls concentrations have been simulated with the kinetic model. The resulting changes in induction times with oxygen pressure at various temperatures are depicted in Figure 9. It has been necessary to use a value of oxygen solubility six times higher for iPP3 than for iPP2 to report the experimental discrepancies. This variability on the oxygen solubility is in satisfactory agreement with the large scattering reported when compiling the data of various authors[41–53] (see Figure 2). All these results constitute a supporting evidence of the impact of oxygen solubility on the iPP thermal oxidation kinetics.

It is noteworthy that the activation energy of oxygen solubility undergoes uncertainty due to large data scattering over a too small interval of temperatures. But, it takes a low value in agreement with our expectations. Since the rate constant k_2 and the coefficient of oxygen solubility are strongly correlated, there is a compensation effect between their respective activation energies. Thus, affecting small activation energy on S_{O2} enables to minimize the value of Ea_2, as expected for very fast reactions (compared with k_4 and k_5). Eventually, Ea_2 was set at 10 kJ mol^{-1}, in agreement with previous studies.[2,64] In addition to the effect of oxygen solubility on its dependence with the oxygen partial pressure, it is also noteworthy that the apparent yield in carbonyl products γ_1^{app} decreases with the oxygen partial pressure (Table V) from a value of 0.5 in oxygen default up to 0.2 in oxygen excess. This variation can be related to the changes in the formation mechanisms of oxidation products, including VOCs, with oxygen partial pressure.[33] This is of particular interest as source of error when determining the critical oxygen pressure from the kinetic curves of carbonyls build-up.

Critical Oxygen Pressure. The dependence of the oxidation behavior with oxygen partial pressure can be materialized by the critical oxygen pressure Pc. This quantity has thus been tentatively determined, by using the analytical relationships reported in Appendix B for all the relevant literature results

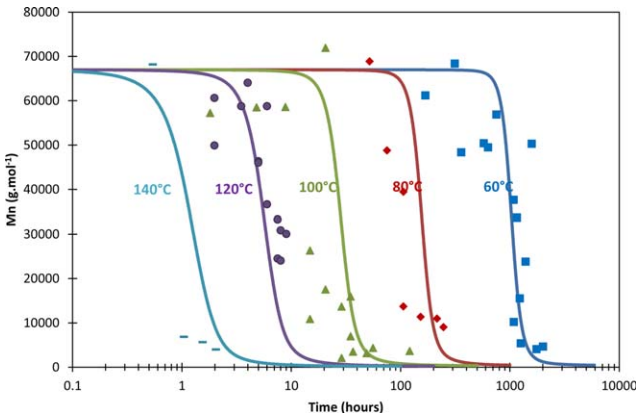

Figure 7. Changes in the number average molecular mass of iPP1 under 0.02 MPa between 60 and 140°C. Symbols: experimental data. Solid lines: kinetic modeling. [Color figure can be viewed in the online issue, which is available at wileyonlinelibrary.com.]

between 40 and 160°C.[12,15,65–68] The resulting Arrhenius graph of the critical oxygen pressure has been plotted in Figure 10.

First, the width of the cluster of Pc values is quite well described by the assumed variability of oxygen solubility. Surprisingly, the theoretical plots show some extrema instead of the expected straight-lines for an Arrhenian behavior. Actually, this singular behavior results from the detail of step (6), considering that peroxy macroradicals can escape from the cage, whose behavior is not Arrhenian anymore. The activation energy of the critical oxygen pressure can be written from eq. (17) as:

$$Ea_{P_c} \approx Ea_2 + Ea_s + Ea_6 - Ea_3 - Ea_5 \qquad (21)$$

When calculating the activation energy of Ea_6 according to eq. (11), values range from 30 to 75 kJ mol^{-1}. Therefore, Ea_{Pc} varies between −16 and 29 kJ mol^{-1} in the temperature range under study. This kind of graph could constitute a good way to check the existence of the cage reaction.

However, it is difficult to conclude on the Arrhenius character of the critical oxygen pressure because of the wide data scatter-

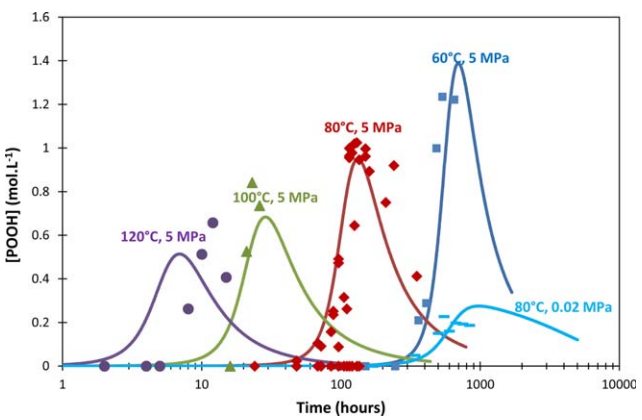

Figure 8. Changes in the hydroperoxydes concentration of iPP2 under 5 MPa between 60 and 140°C and under 0.02 MPa at 80°C. Symbols: experimental data coming from Ref. 3. Solid lines: kinetic modeling.[Color figure can be viewed in the online issue, which is available at wileyonlinelibrary.com.]

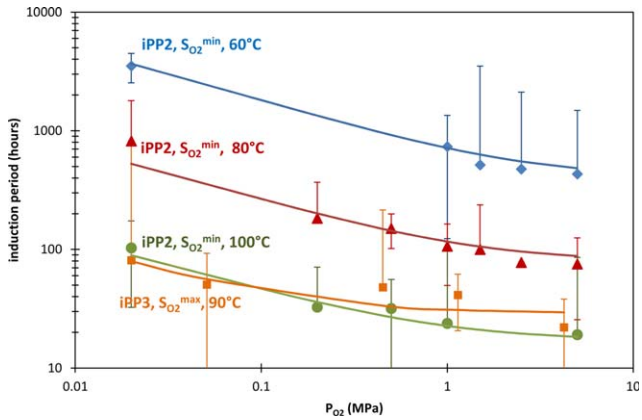

Figure 9. Dependences with oxygen partial pressure of induction time (from carbonyl species) for iPP2 and iPP3 with different coefficients of oxygen solubility (respectively $S_{O2}^{min} = 4.2 \times 10^{-7}$ exp(−6700/RT) and $S_{O2}^{max} = 2.5 \times 10^{-6}$ exp(−6700/RT) mol L^{-1} Pa^{-1}) between 60 and 100°C. Symbols: experimental data. Solid lines: kinetic modeling. [Color figure can be viewed in the online issue, which is available at wileyonlinelibrary.com.]

ing, which is presumably due to questionable methods of treatment for experimental results, in particular:

1. The use of analytical relationships instead of numerical simulation to determine Pc.
2. The mode of calculation of the oxidation criteria which can induce errors when based on carbonyl index[3,12] or mechanical properties[68] instead of oxygen uptake experiments.
3. The use of data sometimes measured at oxygen partial pressures noticeably lower than Pc, thus requiring risky extrapolation to determine Pc. Similarly, these aspects, and particularly the latter, could partly explain that no significant differences in critical oxygen pressure are observed between the various iPPs studied by Bogayevskaya et al.,[15] despite their very different morphological features.

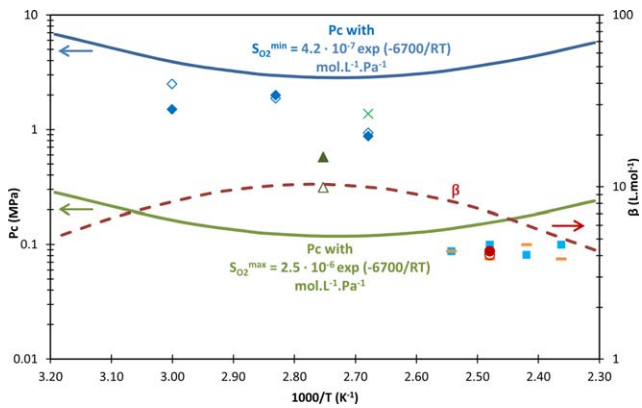

Figure 10. Arrhenius graph of the critical oxygen pressure Pc for boundary values of oxygen solubility (solid lines) and coefficient of oxygen pressure dependence β (dotted line) for iPP between 40 and 160°C. Filled and open symbols apply to the experimental values of Pc determined from induction times and from oxidation rates, respectively: ◇,◆, Richaud et al.[3]; △,▲ Faulkner[12]; ●, ○ Bogayevskaya et al.[15]; ■ Miller et al.[20]; — Reich and Stivala,[123]; ✕ Vink and Fontijn.[68] [Color figure can be viewed in the online issue, which is available at wileyonlinelibrary.com.]

Table V. Changes in the Apparent Yield γ_1^{app} of Carbonyl Products with Oxygen Partial Pressure

Material	Oxygen partial pressure (MPa)	T (°C)	γ_1^{app}
iPP1	0.02	60–140	0.5
iPP2	0.02	60–100	0.5
iPP2	0.2	80–100	0.2
iPP2	0.5	80	0.2
iPP2	1	60	0.15
iPP2	1	80	0.3
iPP2	1	100	0.4
iPP2	1.5	60	0.4
iPP2	1.5	80	0.2
iPP2	1.5	100	0.4
iPP2	2.5	60	0.2
iPP2	5	60–120	0.2
iPP3	0.02	60–90	0.5
iPP3	0.051	90	0.3
iPP3	0.45	90	0.3
iPP3	1.14	90	0.3
iPP3	4.24	60–90	0.3

Values range gradually from 0.5 under ambient pressure to 0.2 in oxygen excess (under 5 MPa).

Consequences of the Variability of S_{O2} on the iPP Oxidation Behavior. The variation of S_{O2} now enables to simulate the whole range of induction times compiled from the literature under 0.1 MPa[6,12,14,17,20,30,31,40,54,56,61,69–93] and 0.02 MPa,[11–20,94–105] except the lowest values attributed to polypropylenes which are atactic, preoxidized or with a high catalyst residues amount (Figure 11). The slope of the Arrhenius graph, i.e. the activation energy predicted by the model, is slightly lower than that given by the global trend of compiled data, but was optimized on the reference polypropylene (iPP1).

Similarly, the variability of the oxygen solubility enables to simulate a larger cluster of maximal oxidation rates among the compilation of literature data[6,16,40,54,56,69,82–85,87,106–108] than the effect of the crystallinity ratio alone (see Figure 12). Moreover, the highest value of solubility, more consistent with the compilation of iPP data than the previous one, does not allow to simulate the upper range of this compilation, particularly above 110°C. This can be related to the additional oxygen consumption through secondary reactions due on the higher reactivity of labile hydrogens from secondary alcohols and ketones compared to methyne sites, as suggested by Mayo. These reactions have not been considered in the kinetic model, thus leading to a slight underestimation of the maximal oxidation rate.[31]

The introduction of variability on the oxygen solubility can be connected with the effect of morphology on the polymer sensitivity to oxidation. Indeed, the induction period was reported to decrease with increasing density and crystallinity ratio,[109,110] crystallites size[15] or annealing temperature[84] as reviewed by Vink.[111] These results, somewhat conflicting in a first approach, could be the consequence of the existence of different iPP crystalline structures. Indeed, iPP crystals can exist in monoclinic (α), hexagonal/trigonal (β), orthorhombic (γ) or smectic/mesomorphic (δ) lattices (see review Ref. 112 for further details). The smectic lattice would be promoted by quenching and characterized by lower crystallinity ratios and smallest spherulithes. In contrast, the more stable (in terms of physical aging) α-monoclinic crystal lattice would be favored by annealing (especially above 90°C) and a low cooling rate, and would be associated to higher crystallinity ratios and coarsest spherulithes. Actually, the former α-monoclinic lattice would oxidize faster than the β-hexagonal or δ-smectic lattices as found by Vieth and Wurth[113] and confirmed in other studies.[114–116]

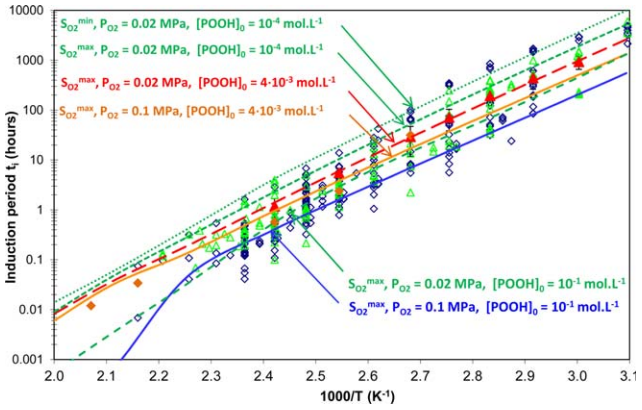

Figure 11. Arrhenius graph of oxidation induction time of iPP between 40 and 200°C. Symbols: Experimental data from several techniques (oxygen uptake, carbonyl index, microcalorimetry, thermogravimetry, or chemiluminescence) under 0.1 (◇) and 0.02 MPa (△) compiled from the literature. Solid and dashed lines apply to simulations made with the indicated values of S_{O2}, P_{O2} and $[POOH]_0$ under 0.1 and 0.02 MPa respectively. The results for iPP1 are depicted in orange and red, respectively. [Color figure can be viewed in the online issue, which is available at wileyonlinelibrary.com.]

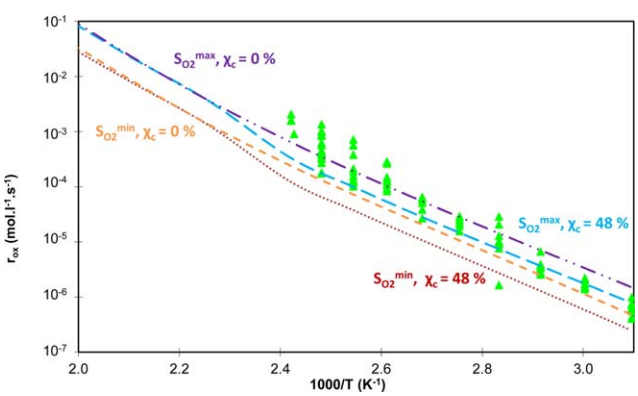

Figure 12. Arrhenius graph of the maximal oxidation rate of iPP between 40 and 230°C under 0.1 MPa. Symbols: Experimental data from oxygen uptake compiled from the literature. Solid lines: simulations made with the indicated values of S_{O2} and χ_c. [Color figure can be viewed in the online issue, which is available at wileyonlinelibrary.com.]

In contrast, Kato et al.[117] observed no correlation between the iPP stability to oxidation and its morphology, and ascribed the discrepancy of stability to differences of molecular order, that is to say tacticity. This assertion was supported by various authors.[118,119] However, it is now well-established that these structural and morphological features are closely intertwined since high isotacticity index would favor crystallization.

CONCLUSION

This work deals with the interrelationship between the oxygen transport properties and rate constants for modeling the iPP thermal oxidation. The resulting general kinetic model was thus calibrated on a reference material (iPP1) and was capable of simulating the concentration changes in primary (e.g. hydroperoxides) and secondary oxidation products such as carbonyl species, but also the changes in molecular masses for different iPPs.

The variability of oxygen solubility was shown to be critical in order to describe the polypropylene thermal oxidation kinetics. Indeed, the current adjustable parameter, namely the initial concentration in hydroperoxides $[POOH]_0$, was unable to report the scattering of iPP oxidation induction times, particularly in oxygen default. In contrast, the introduction of a variability on the oxygen solubility enables to explain the discrepancies of oxygen partial pressure dependences between the three different iPPs under study, as well for induction period as for oxidation rate. The meaning of this latter variability constitutes a key issue. Indeed, it can be attributed to:

- Either morphological difference in terms of lamellar structures. In this case, the variability of the oxygen solubility enables to introduce into the kinetic model the impact of the polymer morphology on the chemistry of oxidation. This option has been considered by default since the variability has been checked to be roughly compatible with the experimental data scattering despite the noticeable uncertainty of measurements.
- Or structural features, in particular the average length of isotactic sequences, which would impact the local reactivity of oxygen with iPP. In this case, the oxygen solubility appears as an apparent and so, an adjustable parameter.

To discriminate between both options, it would be necessary to investigate the coupling between the physical/morphological and chemical aging. In this perspective, it could be relevant to perform specific analyses such as real-time SAXS measurements along the course of oxidation or to perform permeametry measurements on various iPPs of controlled morphologies for instance by using β-nucleating agents. Thus, the challenge would be to propose, in a near future, structure/solubility relationships to reduce the number of remaining empirical steps in the kinetic model.

APPENDIX A: MODEL EQUATIONS, NUMERICAL COMPUTATION, AND RESOLUTION

A SDE can be derived from the CLMS for polypropylene thermal oxidation. However, in the case of relatively thick samples (typically few millimeters thick), oxidation is restricted to superficial layers: indeed, oxygen is the reactant in default in the core of the sample because its diffusion is much slower than its chemical consumption by the chemical reaction. It is thus necessary to introduce the second Fick's law in the SDE to take into account this oxidation control by oxygen diffusion (eqs. A1–A6).

$$\frac{d[P^\bullet]}{dt} = 2k_{1u}[POOH] + k_{1b}[POOH]^2 - k_2[P^\bullet][O_2] + k_3[PO_2^\bullet][PH] - 2k_4[P^\bullet]^2 - k_5[P^\bullet][PO_2^\bullet] + 2k_{6d}[PO^{\bullet\bullet}OP] \quad (A1)$$

$$\frac{d[PO_2^\bullet]}{dt} = k_{1b}[POOH]^2 + k_2[P^\bullet][O_2] - k_3[PO_2^\bullet][PH] - k_5[P^\bullet][PO_2^\bullet] - 2k_{6a}[PO_2^\bullet]^2 \quad (A2)$$

$$\frac{d[POOH]}{dt} = -k_{1u}[POOH] - 2k_{1b}[POOH]^2 + k_3[PO_2^\bullet][PH] + (1-\gamma_5)k_5[P^\bullet][PO_2^\bullet] \quad (A3)$$

$$\frac{d[PH]}{dt} = -2k_{1u}[POOH] - k_{1b}[POOH]^2 - k_3[PO_2^\bullet][PH] + (1-\gamma_4)k_4[P^\bullet]^2 - 2k_{6d}[PO^{\bullet\bullet}OP] \quad (A4)$$

$$\frac{d[PO^{\bullet\bullet}OP]}{dt} = k_{6a}[PO_2^\bullet]^2 - (k_{6b}+k_{6d})[PO^{\bullet\bullet}OP] \quad (A5)$$

$$\partial[O_2]/\partial t = D_{O_2}\,\partial^2[O_2]/\partial z^2 - k_2[P^\bullet][O_2] + k_{6a}[PO_2^\bullet]^2 \quad (A6)$$

where $[P^\bullet]$, $[PO_2^\bullet]$, $[POOH]$, $[PH]$, $[PO^{\bullet\bullet}OP]$ and $[O_2]$ are the respective concentrations of alkyl and peroxy radicals, hydroperoxides, tertiary CH groups, cage paired alkoxy radicals, and oxygen, which are defined at each time t and depth z. D_{O2} is the coefficient of oxygen diffusion in the polymer, here considered as constant and concentration independent.

The SDE admits the following initial conditions:

$$\forall z, \quad t=0,$$

$$[P^\bullet](0,z) = [PO_2^\bullet](0,z) = [PO^{\bullet\bullet}OP](0,z) = 0\,\text{mol L}^{-1} \quad (A7)$$

$$[PH](0,z) = [PH]_0 = 20.3\,\text{mol L}^{-1} \quad \text{(concentration of tertiary CH groups)} \quad (A8)$$

$$[POOH](0,z) = [POOH]_0 = 10^{-5}\text{–}10^{-1}\,\text{mol L}^{-1} \quad (A9)$$

$$\text{and } [O_2](0,z) = Cs \quad (A10)$$

The boundary conditions at the sample edges ($z = 0$ and L) are:

$$\forall\, t > 0, \quad [O_2](t,\ 0) = [O_2](t,\ L) = C_s \quad (A11)$$

where C_s is the oxygen concentration for a material in equilibrium with the atmosphere under a given oxygen partial pressure P_{O_2}. This quantity is assumed to obey the Henry's law:

$$C_s = P_{O_2} \times S_{O_2} \quad (A12)$$

where P_{O_2} is the oxygen partial pressure in the atmosphere and S_{O_2} is the coefficient of oxygen solubility in the polymer.

It means that the sample has reached its equilibrium oxygen concentration C_s elsewhere before starting thermal oxidation. On the contrary, at the transitory state, only the superficial layer is in equilibrium with the surrounding atmosphere, which suggests an immediate dissolution of oxygen in the polymer.

The simultaneous solving of eqs. (A1)–(A6) in space (z) and time (t) with initial and boundary conditions [eqs. (A7)–(A12)]

enables to calculate the local concentration changes in chemical species directly involved in the CLMS, whatever the distance z from the sample surface. The SDE was solved numerically using the ODE15s or ODE23s MATLAB algorithms, which are the recommended semi-implicit methods for stiff problems of chemical kinetics.[120] Yet, it is noteworthy that the SDE only describes phenomena occurring in the amorphous phase where oxygen is dissolved. Therefore, the parameters relative to the local chemistry, such as oxygen consumption and solubility, must be defined in the amorphous phase. On the contrary, parameters describing physical phenomena, such as the oxygen diffusivity, are relative to the whole semi-crystalline polymer. Since oxygen is not soluble in the crystalline phase,[40] the real concentrations for all chemical species have been deduced from their concentrations calculated in the amorphous phase by multiplying them by the volumic fraction of amorphous phase V_a:

$$V_a = (1-\chi_c) \times \frac{\rho_{tot}}{\rho_{am}} \tag{A13}$$

with χ_c the crystallinity ratio, ρ_{am} the density of the amorphous phase (0.85 g cm^{-3}), and ρ_{tot} the density of the semicrystalline polymer (0.91 g cm^{-3}).

At the molten state, the crystallinity ratio is fixed at 0, considering that the liquid state is equivalent to an amorphous phase. Clearly, the kinetic modeling of the thermal oxidation of the semicrystalline polymer at the solid state is based on a homogenization approach at the micron scale.

To compare with experimental data, such as FTIR aging monitoring, average concentrations and global properties throughout the whole sample thickness were calculated by summing the local values calculated in the N-1 computational elementary sublayers:

$$Y_{global}(t) = \frac{1}{N-1}\int_{z=0}^{z=N} Y(z,t)dz \tag{A14}$$

APPENDIX B: ANALYTICAL RELATIONSHIPS FOR DESCRIBING THE OXYGEN PRESSURE DEPENDENCE OF OXIDATION BEHAVIOR

In previous articles,[121] analytical expressions of oxidation rate and oxidation induction times have been derived from the CLMS and the steady state assumption in order to describe the oxygen partial pressure dependence of both physico-chemical quantities. Their respective expressions are reminded just below:

$$\frac{r_{ox}}{r_s} = 2\left(\frac{\beta[O_2]}{1+\beta[O_2]}\right)\left(1-\frac{1}{2}\left(\frac{\beta[O_2]}{1+\beta[O_2]}\right)\right) \tag{B1}$$

and

$$\frac{OIT}{OIT_s} = \left(1+\frac{1}{\beta[O_2]}\right)^{1/2} \tag{B2}$$

where r_s and OIT_s are their respective values in oxygen excess (i.e. close to oxygen saturation):

$$r_s = \frac{k_3^2[PH]^2}{4\ k_6} \tag{B3}$$

and

$$OIT_s = \frac{1+\psi}{k_3[PH]\left(\frac{k_1}{k_6}\right)^{1/2}} \tag{B4}$$

One can plot the curve of both quantities in reduced coordinates:

Figure B1:

$$r_{ox}/r_s = f(\beta[O_2])$$

Figure B2:

$$OIT/OIT_s = f(\beta[O_2])$$

It is clear that both oxidation indicators have clearly different dependences with the oxygen partial pressure. This appendix is thereby dedicated to the the determination of the critical oxygen pressure, delimitating "oxygen excess" from "oxygen default" regimes. Oxygen is considered in excess when its concentration reaches a saturation value in the polymer within an arbitrary tolerance or threshold, that is, when $[O_2] \geq [O_2]_c$ with:

$$[O_2]_c = {}^{K}/_{\beta} = K\ .\ {}^{k_3\ k_5\ [PH]}/_{k_2\ k_6} \tag{B5}$$

In terms of oxygen partial pressure, oxygen excess conditions will be considered as fulfilled when $P_{O2} \geq Pc$, with:

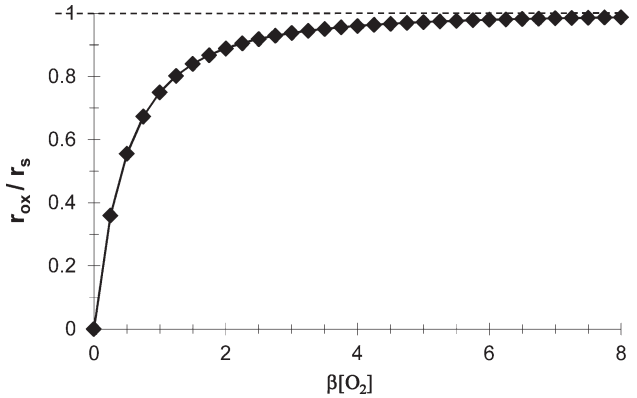

Figure B1. Oxidation rate versus oxygen partial pressure.

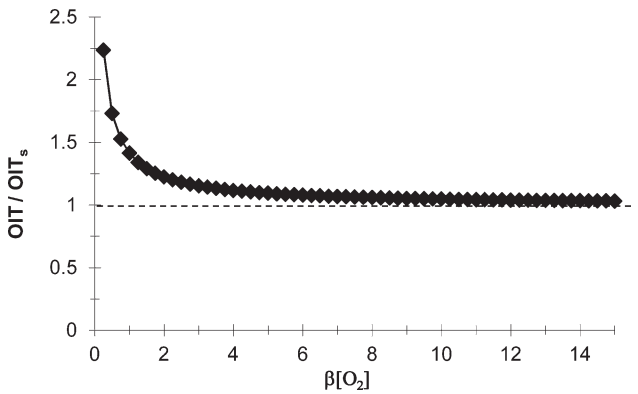

Figure B2. Oxidation induction time versus oxygen partial pressure.

Table BI. Correspondence between Coefficient K and Tolerance Thresholds for Induction Time (κ) and Oxidation Rate (τ)

κ	τ	K
0.7	1.49	0.83
0.75	1.41	1.00
0.8	1.34	1.24
0.85	1.28	1.58
0.9	1.21	2.16
0.91	1.20	2.33
0.92	1.18	2.54
0.93	1.17	2.78
0.94	1.15	3.08
0.95	1.13	3.47
0.96	1.12	4.00
0.97	1.10	4.77
0.98	1.08	6.07
0.99	1.05	9.00

$$\mathrm{Pc} = {}^{[O_2]_c}\Big/_{S_{O_2}} = K \cdot {}^{k_3\ k_5\ [PH]}\Big/_{k_2\ k_6\ S_{O_2}} \tag{B6}$$

From a practical point of view, it appears that K is an arbitrary criterion depending on the oxidation indicator under consideration (r_{ox} or OIT).

For instance, by choosing a tolerance of 5% for both quantities (which is meaningless), it implies that:

$$\beta[O_2] \geq 3.5 \text{ for } r_{ox} \text{ and } \beta[O_2] \geq 9 \text{ for OIT}$$

$$\text{i.e. } K = 3.5 \text{ for } r_{ox} \text{ and } K = 9 \text{ for OIT}$$

These considerations highlight the difficulties encountered for determining Pc from r_{ox} and OIT measurements in a wide range of oxygen partial pressure, being given the numerous sources of experimental errors. Thus, the choice of the K value will be decisive. A more accurate mathematical definition of this parameter is proposed below by using two thresholds:

$$K = \left(\frac{1}{\sqrt{1-\kappa hi}}\right)^{-1} \text{ with } \kappa = r_{ox}/r_s \tag{B7}$$

and

$$K = \left(\tau^2 - 1\right)^{-1} \text{ with } \tau = \mathrm{OIT}/\mathrm{OIT}_s \tag{B8}$$

From these equations, the K values have been determined for both oxidation indicators in Table BI. It is noteworthy that values of Pc depicted in Figure 10 have been determined with $\kappa = 0.8$ and $\tau = 1.34$, both resulting in $K = 1.24$.

REFERENCES

1. Audouin, L.; Gueguen, V.; Tcharkhtchi, A.; Verdu, J. *J. Polym. Sci. Part A: Polym. Chem.* **1995**, *33*, 921.
2. Rincon, R. L. M.; Fayolle, B.; Audouin, L.; Verdu, J. *Polym. Degrad. Stab.* **2001**, *74*, 177.
3. Richaud, E.; Farcas, F.; Bartoloméo, P.; Fayolle, B.; Audouin, L.; Verdu, J. *Polym. Degrad. Stab.* **2006**, *91*, 398.
4. Sarrabi, S.; Colin, X.; Tcharkhtchi, A. *J. Appl. Polym. Sci.* **2010**, *118*, 980.
5. Colin, X.; Audouin, L.; Verdu, J. *Polym. Degrad. Stab.* **2004**, *86*, 309.
6. Gijsman, P.; Hennekens, J.; Vincent, J. *Polym. Degrad. Stab.* **1993**, *39*, 271.
7. Carlsson, D. J.; Wiles, D. M. *J. Macromol. Sci. Polym. Rev.* **1976**, *14*, 65.
8. Audouin, L.; Achimsky, L.; Verdu, J. In Handbook of Polymer Degradation, 2nd ed.; Hamid, S. H., Ed.; Marcel Dekker: New York, **2000**.
9. Colin, X.; Fayolle, B.; Audouin, L.; Verdu, J. *Polym. Degrad. Stab.* **2003**, *80*, 67.
10. Richaud, E.; Colin, X.; Fayolle, B.; Audouin, L.; Verdu, J. *Int. J. Chem. Kinet.* **2008**, *40*, 769.
11. Achimsky, L.; Audouin, L.; Verdu, J.; Rychly, J.; Matisova-Rychla, L. *Polym. Degrad. Stab.* **1997**, *58*, 283.
12. Faulkner, D. L. *Polym. Eng. Sci.* **1982**, *22*, 466.
13. Fayolle, B. PhD thesis, Ecole Nationale Supérieure des Arts et Métiers, Paris, **2001**.
14. Billingham, N. C.; Bott, D. C.; Manke, A. S. Developments in Polymer Degradation; Applied Science: London, **1981**.
15. Bogayevskaya, T. A.; Gromov, B. A.; Miller, V. B.; Monakhova, T. V.; Shlyapnikov, Y. A. *Polym. Sci. USSR* **1972**, *14*, 1741.
16. Boss, C. R.; Chien, J. C. W. *J. Polym. Sci. Part A-1: Polym. Chem.* **1966**, *4*, 1543.
17. Forsstrom, D.; Hamskog, M.; Eriksson, P.; Terselius, B. *Polym. Degrad. Stab.* **2003**, *81*, 81.
18. Gugumus, F. *Polym. Degrad. Stab.* **1996**, *52*, 145.
19. Gugumus, F. *Polym. Degrad. Stab.* **1998**, *62*, 245.
20. Miller, F. A.; Neiman, M. B.; Shlyapnikov, Y. A. *Vysokomolekul. Soedin* **1959**, *1*, 1703.
21. Carlsson, D. J.; Brousseau, R.; Wiles, D. M. *Polym. Degrad. Stab.* **1986**, *15*, 67.
22. Carlsson, D. J.; Lacoste, J. *Polym. Degrad. Stab.* **1991**, *32*, 377.
23. Rutherford, S. W.; Do, D. D. *Adsorption* **1997**, *3*, 283.
24. Bolland, J. L. *Proc. R. Soc. London Ser. A* **1946**, *186*, 218.
25. Bolland, J. L.; Gee, G. *Trans. Faraday Soc.* **1946**, *42*, 236.
26. Bolland, J. L.; Gee, G. *Trans. Faraday Soc.* **1946**, *42*, 244.
27. Tobolsky, A. V.; Metz, D. J.; Mesrobian, R. B. *J. Am. Chem. Soc.* **1950**, *72*, 1942.
28. Tobolsky, A. V.; Norling, P. M.; Frick, N. H.; Yu, H. *J. Am. Chem. Soc.* **1964**, *86*, 3925.
29. Somersall, A. C.; Guillet, J. E. In Polymer Stabilization and Degradation; Klemchuk, P. P., Ed.; ACS Symposium series; American Chemical Society: Washington, **1985**; Chapter 16, *280*, pp 211.
30. Sarrabi, S.; Colin, X.; Tcharkhtchi, A. *J. Appl. Polym. Sci.* **2008**, *110*, 2030.

31. Reich, L.; Stivala, S. S. Elements of Polymer Degradation; McGraw-Hill: New York, **1971**; Chapter 5, pp 164.
32. Khelidj, N.; Colin, X.; Audouin, L.; Verdu, J.; Monchy-Leroy, C.; Prunier, V. *Polym. Degrad. Stab.* **2006**, *91*, 1598.
33. François-Heude, A.; Richaud, E.; Leprovost, J.; Heninger, M.; Mestdagh, H.; Desnoux, E.; Colin, X. *Polym. Test.* **2013**, *32*, 907.
34. Saito, O. *J. Phys. Soc. Jpn.* **1958**, *13*, 198.
35. Kelen, T.; Iring, M.; Tüdo, s. F. *Eur. Polym. J.* **1976**, *12*, 35.
36. Korcek, S.; Chenier, J. H. B.; Howard, J. A.; Ingold, K. U. *Can. J. Chem.* **1972**, 2285.
37. Gillen, K. T.; Wise, J.; Clough, R. L. *Polym. Degrad. Stab.* **1995**, *47*, 149.
38. Colin, X.; Richaud, E.; Verdu, J.; Monchy-Leroy, C. *Radiat. Phys. Chem.* **2010**, *79*, 365.
39. Richaud, E.; Farcas, F.; Fayolle, B.; Audouin, L.; Verdu, J. *Polym. Degrad. Stab.* **2007**, *92*, 118.
40. Knight, J. B.; Calvert, P. D.; Billingham, N. C. *Polymer* **1985**, *26*, 1713.
41. Beltrame, P. L.; Citterio, C.; Testa, G.; Seves, A. *J. Appl. Polym. Sci.* **1999**, *74*, 1941.
42. Denisov, E. T.; Afanas'ev, I. B. Oxidation and Antioxidants in Organic Chemistry and Biochemistry; CRC Press, Taylor and Francis: Boca Raton, **2006**.
43. Kiryushkin, S. G. Dissertation, Institute Chemical Physics: Moscow, **1975**.
44. Kurek, M.; Klepac, D.; Ščetar, M.; Galić, K.; Valić, S. k.; Liu, Y.; Yang, W. *Polym. Bull.* **2011**, *67*, 1293.
45. Lin, Y. J.; Dias, P.; Chen, H. Y.; Chum, S.; Hiltner, A.; Baer, E. *Polym. Eng. Sci.* **2008**, *48*, 642.
46. Lin, Y. J.; Dias, P.; Chen, H. Y.; Hiltner, A.; Baer, E. *Polymer* **2008**, *49*, 2578.
47. Somlai, L. S.; Liu, R. Y. F.; Landoll, L. M.; Hiltner, A.; Baer, E. *J. Polym. Sci. Part B: Polym. Phys.* **2005**, *43*, 1230.
48. Thorlaksen, P.; Abildskov, J.; Kontogeorgis, G. M. *Fluid Phase Equilib.* **2003**, *211*, 17.
49. Villaluenga, J. P. G.; Khayet, M.; Lopez-Manchado, M. A.; Valentin, J. L.; Seoane, B.; Mengual, J. I. *Eur. Polym. J.* **2007**, *43*, 1132.
50. Stannet, V. In Diffusion in Polymers; Crank, J., Park, J. S., Eds.; Academic Press: New York, **1968**; Chapter 2, p 41.
51. Van Krevelen, D. W.; Hoftyzer, P. J. Properties of Polymers; Elsevier: Amsterdam, **1976**.
52. Gutiérrez, G. G. PhD thesis, Arts et Metiers ParisTech: Paris, **2010**.
53. Mani, R.; Singh, R. P.; Sivaram, S.; Lacoste, J.; Lemaire, J. *J. Macromol. Sci. Pure Appl. Chem.* **1996**, *33*, 783.
54. Tüdos, F.; Iring, M.; Kelen, T. International Conference on Advances in the Stabilization and Controlled Degradation of Polymers, Lucerne, Switzerland, A.V. Patsis, New York, **1985**.
55. Achimsky, L. PhD thesis, Université Pierre et Marie-Curie (Paris VI): Paris, **1996**.
56. Iring, M.; László-Hedvig, S.; Tüdos, F.; Kelen, T. *Polym. Degrad. Stab.* **1983**, *5*, 467.
57. Billingham, N. C. *Die Makromol. Chem. Macromol. Symp.* **1989**, *28*, 145.
58. Tüdős, F.; Iring, M. *Acta Polym.* **1988**, *39*, 19.
59. Fayolle, B.; Audouin, L.; Verdu, J. *Polymer* **2004**, *45*, 4323.
60. Kamiya, Y.; Niki, E. In Aspects of Degradation and Stabilization of Polymers; Jellinek, H., Ed.; Elsevier Science: New York, **1978**.
61. Celina, M.; George, G. A. *Polym. Degrad. Stab.* **1993**, *40*, 323.
62. Goss, B. G. S.; Blakey, I.; Barry, M. D.; George, G. A. *Polym. Degrad. Stab.* **2001**, *74*, 523.
63. Goss, B. G. S.; Nakatani, H.; George, G. A.; Terano, M. *Polym. Degrad. Stab.* **2003**, *82*, 119.
64. Stivala, S. S.; Kimura, J.; Gabbay, S. M. In Degradation and Stabilization of Polyolefins; Allen, N. S., Ed.; Appl. Sci. Publ.: London, **1983**; Chapter 3.
65. Miller, V. B.; Neiman, M. B.; Shliapnikov, I. A. *Polym. Sci. USSR* **1961**, *2*, 129.
66. Reich, L.; Stivala, S. S. Autoxidation of hydrocarbons and polyolefins: Kinetics and mechanisms; Marcel Dekker, Inc.: New York, **1969**.
67. Richaud, E. PhD thesis, Arts et Métiers ParisTech: Paris, **2006**.
68. Vink, P.; Fontijn, H. F. N. *Geotext. Geomemb.* **2000**, *18*, 333.
69. Gijsman, P. Ph.D thesis, Technische Universiteit Eindhoven, Netherlands, **1994**, p 176.
70. Mowery, D. M.; Assink, R. A.; Derzon, D. K.; Klamo, S. B.; Clough, R. L.; Bernstein, R. *Macromolecules* **2005**, *38*, 5035.
71. Oswald, H. J.; Turi, E. *Polym. Eng. Sci.* **1965**, *5*, 152.
72. Richters, P. *Macromolecules* **1970**, *3*, 262.
73. Rychly, J.; Matisova-Rychla, L.; Tiemblo, P.; Gomez-Elvira, J. *Polym. Degrad. Stab.* **2001**, *71*, 253.
74. Ahlblad, G.; Gijsman, P.; Terselius, B. r.; Jansson, A.; Möller, K. *Polym. Degrad. Stab.* **2001**, *73*, 15.
75. Celina, M.; George, G. A. *Polym. Degrad. Stab.* **1995**, *50*, 89.
76. Gijsman, P.; Verdun, F. *Polym. Degrad. Stab.* **2001**, *74*, 533.
77. Matisova-Rychla, L.; Rychly, J. *Polym. Degrad. Stab.* **2000**, *67*, 515.
78. Matisova-Rychla, L.; Rychly, J.; Verdu, J.; Audouin, L.; Csomorova, K. *Polym. Degrad. Stab.* **1995**, *49*, 51.
79. Schwarz, T.; Steiner, G.; Koppelmann, J. *J. Therm. Anal.* **1989**, *35*, 481.
80. Reich, L.; Jadrnicek, B. R.; Stivala, S. S. *J. Polym. Sci. Part A-1: Polym. Chem.* **1971**, *9*, 231.
81. Celina, M.; George, G. A.; Billingham, N. C. *Polym. Degrad. Stab.* **1993**, *42*, 335.
82. Hansen, R. H.; Russell, C. A.; De Benedictis, T.; Martin, W. M.; Pascale, J. V. *J. Polym. Sci. Part A: Gen. Pap.* **1964**, *2*, 587.

83. Iring, M.; László-Hedvig, S.; Barabás, K.; Kelen, T.; Tüdos, F. *Eur. Polym. J.* **1978**, *14*, 439.
84. Rapoport, N. Y.; Berulava, S. I.; Kovarskii, A. L.; Musayelyan, I. N.; Yershov, Y. A.; Miller, V. B. *Polym. Sci. USSR* **1975**, *17*, 2901.
85. Rapoport, N. Y.; Livanova, N. M.; Miller, V. B. *Polym. Sci. USSR* **1976**, *18*, 2336.
86. Zlatkevich, L. *Polym. Eng. Sci.* **1984**, *24*, 1421.
87. Meltzer, T. H.; Kelley, J. J.; Goldey, R. N. *J. Appl. Polym. Sci.* **1960**, *3*, 84.
88. Matisova-Rychla, L.; Rychly, J. In Polymer Durability; Advances in Chemistry Series, Clough, R. L., Billingham, N. C., Gillen, K. T., Eds; American Chemical Society: Washington, **1996**; Chapter 12, *249*, pp 175.
89. Celina, M.; George, G. A.; Billingham, N. C. In Polymer Durability: Degradation, Stabilization, and Lifetime Prediction; Advances in Chemistry Series, Clough, R. L., Billingham, N. C., and Gillen, K. T., Eds.; American Chemical Society: Washington, **1996**; Chapter 11, *249*, pp 159.
90. George, G. A.; Celina, M. In Handbook of Polymer Degradation, 2nd ed.; S. Halim Hamid, Marcel Dekker, inc. Ed.; New York, **2000**; Chapter 7, pp. 277.
91. Kato, M.; Osawa, Z. *Polym. Degrad. Stab.* **1999**, *65*, 457.
92. Setnescu, R.; Jipa, S.; Osawa, Z. *Polym. Degrad. Stab.* **1998**, *60*, 377.
93. Bergenudd, H.; Eriksson, P.; DeArmitt, C.; Stenberg, B.; Malmström Jonsson, E. *Polym. Degrad. Stab.* **2002**, *76*, 503.
94. Hawkins, W. L.; Matreyek, W.; Winslow, F. H. *J. Polym. Sci.* **1959**, *41*, 1.
95. Eriksson, P.; Stenberg, B.; Reitberger, T.; Forsström, D. *Polym. Test.* **2003**, *22*, 915.
96. Lemaire, J.; Gardette, J.-L.; Lacoste, J.; Delprat, P.; Vaillant, D. In Polymer Durability; Advances in Chemistry Series, Clough R. L., Billingham N. C., Gillen K.T., Eds; American Chemical Society: Washington, **1996**; Chapter 35, *249*, p 577.
97. Henman, J. T. In Developments in polymer degradation; Vol. 6 Grassie, E., Ed.; Elsevier Applied Science: London, **1985**.
98. Osawa, Z.; Shibamiya, T.; Matsuzaki, K. *J. Soc. Chem. Ind. Japan* **1968**, *71*, 552.
99. Scott, G.; Yusoff, M. F. *Eur. Polym. J.* **1980**, *16*, 497.
100. Al-Malaika, S. *Polym. Degrad. Stab.* **1991**, *34*, 1.
101. Al-Malaika, S.; Scott, G.; Huczkowski, P. *Polym. Degrad. Stab.* **1984**, *7*, 95.
102. Tiemblo, P.; Manuel Gòmez-Elvira, J.; Teyssedre, G.; Massines, F.; Laurent, C. *Polym. Degrad. Stab.* **1999**, *65*, 113.
103. Matisova-Rychla, L.; Rychy, J.; Vavrekova, M. *Eur. Polym. J.* **1978**, *14*, 1033.
104. Jipa, S.; Setnescu, R.; Setnescu, T.; Zaharescu, T. *Polym. Degrad. Stab.* **2000**, *68*, 159.
105. Billingham, N. C.; Calvert, P. D. In Developments in Polymer stabilisation, Vol 3; Scott, G., Ed.; Applied Science: London, **1980**.
106. Mikheev, Y. A.; Guseva, L. N.; Zaikov, G. E. *Polym. Degrad. Stab.* **1999**, *63*, 509.
107. Iring, M.; Laszlo-Hedvig, S.; Kelen, T.; Tudos, F.; Fuzes, L.; Gamey, G.; Bodor, G. *J. Polym. Sci.* **1976**, *57*, 55.
108. Rapoport, N. Y.; Goniashvili, A. S.; Akutin, M. S.; Miller, V. B. *Vysokomol. Soed.* **1979**, *21A*, 2071.
109. McTigue, F. H.; Blumberg, M. *Mod. Plast.* **1967**, *44*, 145.
110. Vink, P. *J. Appl. Polym. Sci.* **1979**, *35*, 265.
111. Vink, P. In Degradation and Stabilisation of Polyolefins; Allen, N. S., Ed.; Applied Science Publishers: London, **1983**.
112. Brückner, S.; Meille, S. V.; Petraccone, V.; Pirozzi, B. *Prog. Polym. Sci.* **1991**, *16*, 361.
113. Vieth, W.; Wuerth, W. F. *J. Appl. Polym. Sci.* **1969**, *13*, 685.
114. Nishimoto, S.; Kagiya, T.; Watanabe, Y.; Kato, M. *Polym. Degrad. Stab.* **1986**, *14*, 199.
115. Obadal, M.; Cermak, R.; Raab, M.; Verney, V.; Commereuc, S.; Fraïsse, F. *Polym. Degrad. Stab.* **2005**, *88*, 532.
116. Obadal, M.; Cermak, R.; Raab, M.; Verney, V.; Commereuc, S.; Fraïsse, F. *Polym. Degrad. Stab.* **2006**, *91*, 459.
117. Kato, Y.; Carlsson, D. J.; Wiles, D. M. *J. Appl. Polym. Sci.* **1969**, *13*, 1447.
118. Nakatani, H.; Suzuki, S.; Tanaka, T.; Terano, M. *Polymer* **2005**, *46*, 12366.
119. Suzuki, S.; Nakamura, Y.; Hasan, A. T. M. K.; Liu, B.; Terano, M.; Nakatani, H. *Polym. Bull.* **2005**, *54*, 311.
120. Hairer, E.; Wanner, G. Stiff and Differential-Algebraic Problems. Series in Computational Mathematics, Springer: Berlin, **1996**.
121. Verdu, J.; Colin, X.; Audouin, L.; Rychly, J.; Matisova-Rychla, L. *Polym. Degrad. Stab.* **2006**, *91*, 1387.
122. Kiryushkin, S. G.; Shlyapnikov, Y. A. *Polym. Degrad. Stab.* **1989**, *23*, 185 1989.
123. Reich, L.; Stivala, S. S. Auto-oxidation of Hydrocarbons and Polyolefins, Kinetics and Mechanisms; Marcel Dekker: New York, **1969**; Chapter 8.
124. Evans, J. M. *Polym. Eng. Sci.* **1973**, *13*, 401.
125. Yau, W. W.; Kirkland, J. J.; Bly, D. D. Modern Size-Exclusion Liquid Chromatography: Practice of Gel Permeation and Gel Filtration Chromatography, 2nd ed.; John Wiley and Sons, inc.: Hoboken, **1979**.
126. Mori, S.; Barth, H. G. Size Exclusion Chromatography; Springer: Berlin, **1999**.